Structural Features of Titanate Nanotubes/Nanobelts Revealed by Raman, X-ray Absorption Fine Structure and Electron Diffraction Characterizations

Renzhi Ma,*,†,‡ Katsutoshi Fukuda,† Takayoshi Sasaki,† Minoru Osada,† and Yoshio Bando‡

Soft Chemistry Group, Advanced Materials Laboratory and International Center for Young Scientists (ICYS), National Institute for Materials Science, Namiki 1-1, Tsukuba, Ibaraki 305-0044, Japan

Received: December 15, 2004; In Final Form: February 2, 2005

High-purity nanotubes and nanobelts could be controllably obtained in hydrothermal treatments of anatase TiO_2 in concentrated NaOH solution depending on treating temperature and duration. Their structural features were studied employing X-ray diffraction, Raman, X-ray absorption fine structure, and electron diffraction characterizations. The results reveal that both the nanotubes and nanobelts might be of layered titanate structure. The similarity and difference among the nanotubes/nanobelts and other bulk titanates represented by trititanate $H_2Ti_3O_7$ and lepidocrocite-type $H_{0.7}Ti_{1.825}\square_{0.175}O_{4.0}\cdot H_2O$ were also presented.

Introduction

It is well-known that various alkali metal titanates represented by the chemical formula $A_2Ti_nO_{2n+1}$ (A = alkali metal ion or proton, $n = 2-9$) have their own crystal structures of layered or tunnel-type.[1−10] Particularly, $A_2Ti_nO_{2n+1}$ ($n = 3, 4, 5$) exhibits a monoclinic lattice with parallel corrugated layers of edge-sharing TiO_6 octahedra stepped by every nth octahedra.[1−5] On the other hand, a peculiar lepidocrocite (γ-FeOOH)-type titanate of typical composition $Cs_xTi_{2-x/4}\square_{x/4}O_4$ ($x = 0.7$; $\square$ = vacancy) has a similar layer structure except for the absence of stepped architecture. In other words, the lepidocrocite-type host layer is stepped by an infinite width to produce a continuous and planar two-dimensional array.[11−14] Since these titanates show excellent ion-exchange ability and photocatalytic activities, they have received extensive investigation and may be applied to photocatalysis, photoluminescence, and dye-sensitized solar cells.

Recently, of particular interest is a hydrothermal method to obtain TiO_2-derived nanotubes.[15−20] The nanotube structure is widely accepted as the scrolling of an exfoliated TiO_2-derived nanosheet into a hollow multiwall nanotube with spiral cross section though the crystallographic descriptions were varied from tetragonal anatase,[19] to monoclinic $H_2Ti_3O_7$,[17,18] or orthorhombic lepidocrocite-type $H_{0.7}Ti_{1.825}\square_{0.175}O_{4.0}\cdot H_2O$,[20] etc.[21] The controversy still goes on. In general, the titanate nanotubes can be almost routinely obtained. However, nonhollow nanofibers (nanoribbons) were also reported in some apparently similar hydrothermal procedures.[22] It is thus important to reveal the effect of hydrothermal synthetic conditions on the morphology and their structural similarity/difference. It is also of interest to compare the structure of the hydrothermally synthesized nanomaterials with those of known titanates through microscopic and spectroscopic characterizations.

The effect of hydrothermal conditions on product morphologies was investigated. The synthesized products have been characterized as hollow nanotubes and nonhollow nanofibers (nanobelts) depending on applied hydrothermal temperature and duration. As revealed by Raman, X-ray absorption fine structure (XAFS), and electron diffraction (ED), the structures of the nanotubes and nanobelts both appear to be layered titanates.

Experimental Section

The well-known hydrothermal method was employed for the synthesis.[16,20] Commercial anatase TiO_2 powders (1.5−2 g) were dispersed in an aqueous solution of NaOH (5−10 mol dm^{-3}, 40 cm^3) and charged into a Teflon-lined autoclave. The autoclave was oven-heated at 110−190 °C for 12 h to 1 week. The precipitate was filtrated and washed repeatedly with copious deionized water and diluted HCl/HNO_3. Final products were obtained by air-drying.

For comparison, other bulk titanates of $Na_2Ti_3O_7$, $K_2Ti_4O_9$, $Cs_2Ti_5O_{11}$, and $Cs_{0.7}Ti_{1.825}\square_{0.175}O_4$ were prepared by conventional solid-state calcinations of stoichiometric mixtures of anatase TiO_2 and A_2CO_3 (A = Na, K, Cs), respectively.[1−5,11,12] The synthesized bulk titanates were treated with 1 mol dm^{-3} HCl to be converted into their protonic forms of $H_2Ti_3O_7$, $H_2Ti_4O_9\cdot 1.2H_2O$, $H_2Ti_5O_{11}\cdot 3H_2O$, and $H_{0.7}Ti_{1.825}\square_{0.175}O_{4.0}\cdot H_2O$ (hereafter they are abbreviated as Ti_3O_7, Ti_4O_9, Ti_5O_{11}, and lepidocrocite). Exfoliation of the protonic titanates was performed by reaction with a tetrabutylammonium hydroxide solution ($(C_4H_9)_4NOH$). In a typical procedure, 0.4 g of the protonic titanate was immersed in 100 cm^3 of the aqueous $(C_4H_9)_4NOH$ solution and the mixture was shaken for 2 weeks.[13] Except Ti_3O_7, where it is difficult to achieve the exfoliation, Ti_4O_9, Ti_5O_{11}, and lepidocrocite were readily exfoliated into nanosheets of single elemental-layer thickness in colloidal suspensions.[14] A drop of the colloidal suspensions containing the single-layer nanosheets was transferred to a carbon-coated copper grid for microscopic characterizations.

The products were observed by a scanning electron microscope (SEM, JEOL SM-67F) and a field emission JEM-3000F (JEOL) high-resolution transmission electron microscope (HR-TEM) operated at 300 kV. X-ray diffraction (XRD) patterns were collected on a Rigaku Rint-2000 diffractometer with monochromatized Cu Kα irradiation ($\lambda = 0.15405$ nm). Raman spectra were measured with the 514.5 nm line from an Ar^+ laser (~0.1 mW). The backward scattering light was collected

* Address correspondence to this author. E-mail: ma.renzhi@nims.go.jp.
† Soft Chemistry Group, Advanced Materials Laboratory.
‡ International Center for Young Scientists (ICYS).

10.1021/jp044282r CCC: $30.25
Published on Web 03/11/2005

by a subtractive triple spectrometer (Jobin-Yvon T64000) equipped with a liquid nitrogen cooled charge-couple-device detector.

X-ray absorption near-edge structure (XANES) and extended X-ray absorption fine structure (EXAFS) for the Ti−K edge were measured at the Photon Factory BL-12C in the Institute of Materials Science, High Energy Accelerator Research Organization (KEK−PF). The samples were pelleted with BN powders as the binder. Spectra were recorded in transmission mode from 4660 to 5968 eV for the Ti edge with an interval of 0.6 eV. The EXAFS oscillations $\chi(k)$ (where k is the photoelectron momentum) were extracted from the spectra by using a spline-smoothing method performed with the EXAFS analysis program RIGAKU REX2000 (version 2.3.2). The radial distribution of atoms (RDA) function was calculated from the EXAFS spectra in $k^3\chi(k)$ by Fourier transform (FT).

Results and Discussion

In our experiments, the NaOH concentration of the solution in the range 5−10 mol dm^{-3} did not impose significant impact on the morphology of final products. On the other hand, the morphology was substantially affected by both the hydrothermal treatment temperature and duration period. The combination of a hydrothermal treatment temperature 130−150 °C and a time period 24−72 h gave the best results regarding the nanotube yield and purity (Figure 1a). The inset is a high magnification image of an individual nanotube clearly exhibiting a hollow core and a few (3−5) wall layers on both sides. At a lower treating temperature such as 110 °C and short duration ∼12 h, unreacted TiO_2 particles were apparent (Figure 1b). The increase in hydrothermal temperature was found to facilitate the formation of nonhollow nanofibers. Despite containing some nanotubes, the samples obtained at high temperature (170∼190 °C) and prolonged duration (72 h to 1 week) actually are comprised of abundant nanofibers (Figure 1c,d). The width of the nanofibers is usually 100−300 nm, significantly larger than the nanotube diameter (8−12 nm). The thickness of the nanofibers is usually very thin as judged from TEM contrast, exhibiting a morphology similar to that of nanobelts (hereafter the nanofibers are specifically denoted as nanobelts). It is noteworthy that further treatment of nanotubes in concentrated NaOH solution at temperatures above 170 °C also produced abundant nanobelts. This indicates that the temperature parameter plays a determining role regarding the product morphology.

Figure 2 compares the typical XRD patterns of nanotubes (130 °C, 48 h) and nanobelts (170 °C, 1 week). Both patterns feature a prominent peak at $2\theta \sim 10°$, reflecting a d spacing of ∼0.9 nm, which is a diagnostic gallery spacing for the layered protonic titanates. If an orthorhombic lepidocrocite-type titanate is assumed, the peaks in the patterns can be as assigned as reflections of the basal inter-layer (0k0) series (i.e., (020), (040)), and in-layer (200) and (002). Likewise, if monoclinic stepped titanates of $A_2Ti_nO_{2n+1}$ (n = 3, 4, 5) are considered, the peaks might be ascribed as basal reflections of (h00) (i.e.; (200), (400)) together with in-layer (020) and (00l) ($l = 2n$, n = number of stepped octahedra). As an example, the indices of the patterns to the lepidocrocite titanate structure are shown in Figure 2. The crystallinity of the nanobelts appears somewhat better than that of the nanotubes regarding the sharpness of diffraction peaks and appearance of a high-order basal reflection peak.

Raman spectra of nanotubes and nanobelts are shown in Figure 3. They are almost identical, displaying very broad bands near 145, 195, 280, 450, 640 (700), and 920 cm^{-1}. According to the literature, anatase TiO_2 has six Raman ($A_{1g} + 2B_{1g} + 3E_g$) active modes at 147, 198, 398, 515, 640, and 796 cm^{-1} and rutile TiO_2 has four active modes $A_{1g} + B_{1g} + B_{2g} + E_g$ located at 144, 448, 612, and 827 cm^{-1}, respectively.[23] The spectra of nanotubes/nanobelts are apparently different from that of either the anatase or the rutile phase although some peaks do appear in the vicinities of the above-mentioned active modes due to the TiO_2-derived origin. Our group has previously reported the Raman spectrum of protonic lepidocrocite $H_{0.7}Ti_{1.825}\square_{0.175}O_4$ (spectrum c in Figure 3).[24] The number of observed modes agrees fairly well with the space group theoretical analysis of lepidocrocite titanate, which yields nine ($3A_g + 3B_{2g} + 3B_{3g}$) modes. The spectra of the nanotubes/nanobelts indeed show very similar peak positions and profiles to the protonic lepidocrocite titanate. On the other hand, the

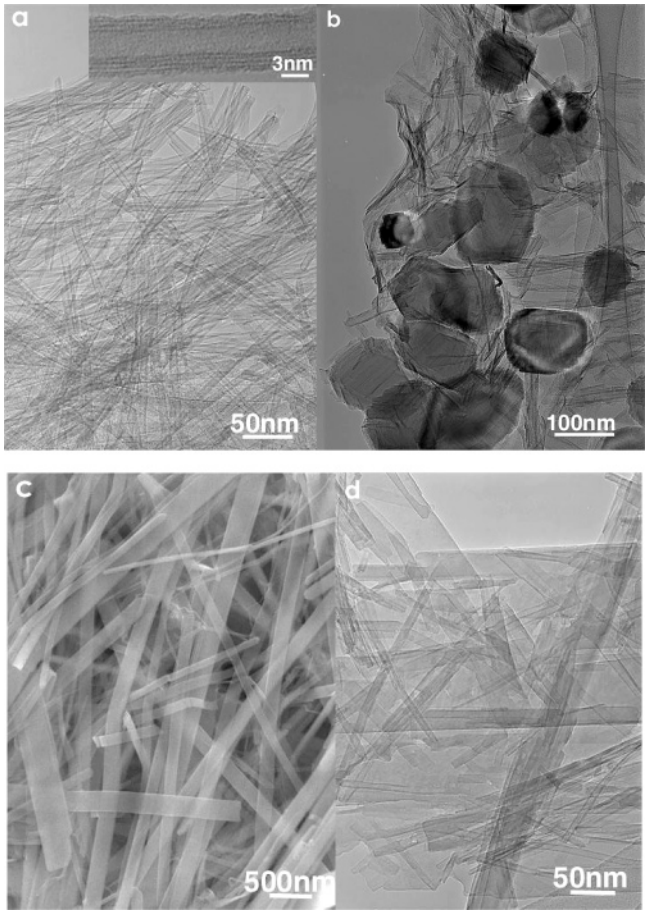

Figure 1. Products synthesized in different hydrothermal procedures. (a) TEM image of high-purity nanotubes obtained with optimal combination of treating temperature and duration. (Inset) High magnification image of an individual nanotube showing an apparent hollow core and a few wall layers on both sides. (b) Residual anatase particles are obvious when low treating temperature and short duration are employed.; (c, d) SEM and TEM images of abundant nanobelts obtained at high temperature above 170 °C.

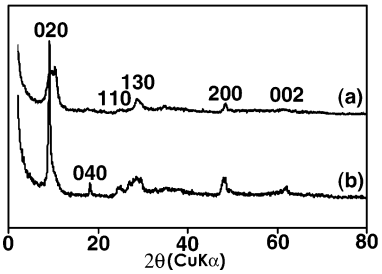

Figure 2. XRD spectra of (a) nanotubes and (b) nanobelts.

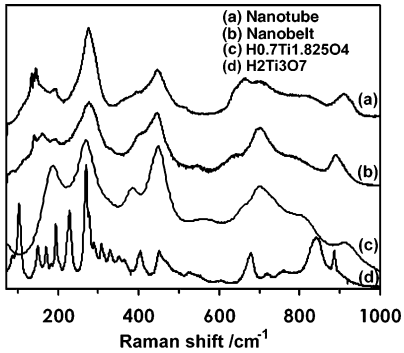

Figure 3. Raman spectra of (a) nanotubes and (b) nanobelts in comparison with (c) $H_{0.7}Ti_{1.825}\square_{0.175}O_4$ and (d) $H_2Ti_3O_7$.

first Raman measurement for $Na_2Ti_3O_7$ was made by Bamberger et al.[25] For comparison, the spectrum of our $H_2Ti_3O_7$ sample is also shown as spectrum d in Figure 3. The notable features of the $Na_2Ti_3O_7/H_2Ti_3O_7$ are the abundant sharp peaks at the lower wavenumber regime of 100−400 cm^{-1} and a characteristic peak near ~850 cm^{-1}, which are absent in the spectra of nanotubes/nanobelts. The greater number of active modes in $Na_2Ti_3O_7/H_2Ti_3O_7$ is likely to reflect the lower symmetry of this stepped titanate than that of lepidocrocite-type. Unfortunately, there are few reports relating directly the Raman peaks to specific active modes in layered titanates.[26,27] Kim et al. investigated the formation of the sodium titanate hydrogel layer on the surface of Ti metal treated in NaOH.[26] They ascribed the appearance of Raman peaks at near 440 and 600 cm^{-1} to the Ti−O bending and stretching vibration involving six-coordinated titanium and three-coordinated oxygen. Kudo et al.[27] reported the Raman spectra of layered cesium titanates of $Cs_2Ti_nO_{2n+1}$ (n = 2, 5) and lepidocrocite-type (denoted as $Cs_2Ti_6O_{13}$ therein). They assigned the peaks at 850−950 cm^{-1} to the stretching modes of Ti−O bonds that stick out into the interlayer space. The Raman features of the nanotubes/nanobelts may be roughly regarded as a reflection of the six-coordinated layered titanate structure. The exact assignment of the Raman spectra is still not available.

The XANES spectra of nanotubes/nanobelts, lepidocrocite titanate, and stepped titanates of Ti_3O_7, Ti_4O_9, and Ti_5O_{11} are compared in Figure 4a. All the spectra exhibit a pre-edge feature consisting of multiple peaks labeled as A1, A2, A3, and B in the energy region of 4964−4974 eV (see enlarged region in Figure 4b), which was followed by white line peaks C1, C2, and D (4983−5003 eV).[28] The pre-edge multiple peaks can be assigned to forbidden transitions from the core 1s level to unoccupied 3d states of a Ti^{4+}. It is known that the profile is highly dependent on the degree of the distortion of TiO_6 octahedron. In Figure 4b, the intensity profiles of A3 are notably different for Ti_3O_7 and lepidocrocite. And the A3 feature of nanotubes/nanobelts appears closer to that for lepidocrocite than Ti_3O_7. The white line region in the XANES features arises from dipole-allowed transitions from the core 1s to unoccupied 4p states. The white line characteristics of C1 and C2 for different titanates are compared in Figure 4c. As a common feature, stepped titanates of Ti_3O_7, Ti_4O_9, and Ti_5O_{11} show two excitation peaks (C1, C2) located around 4984.5 and 4989.5

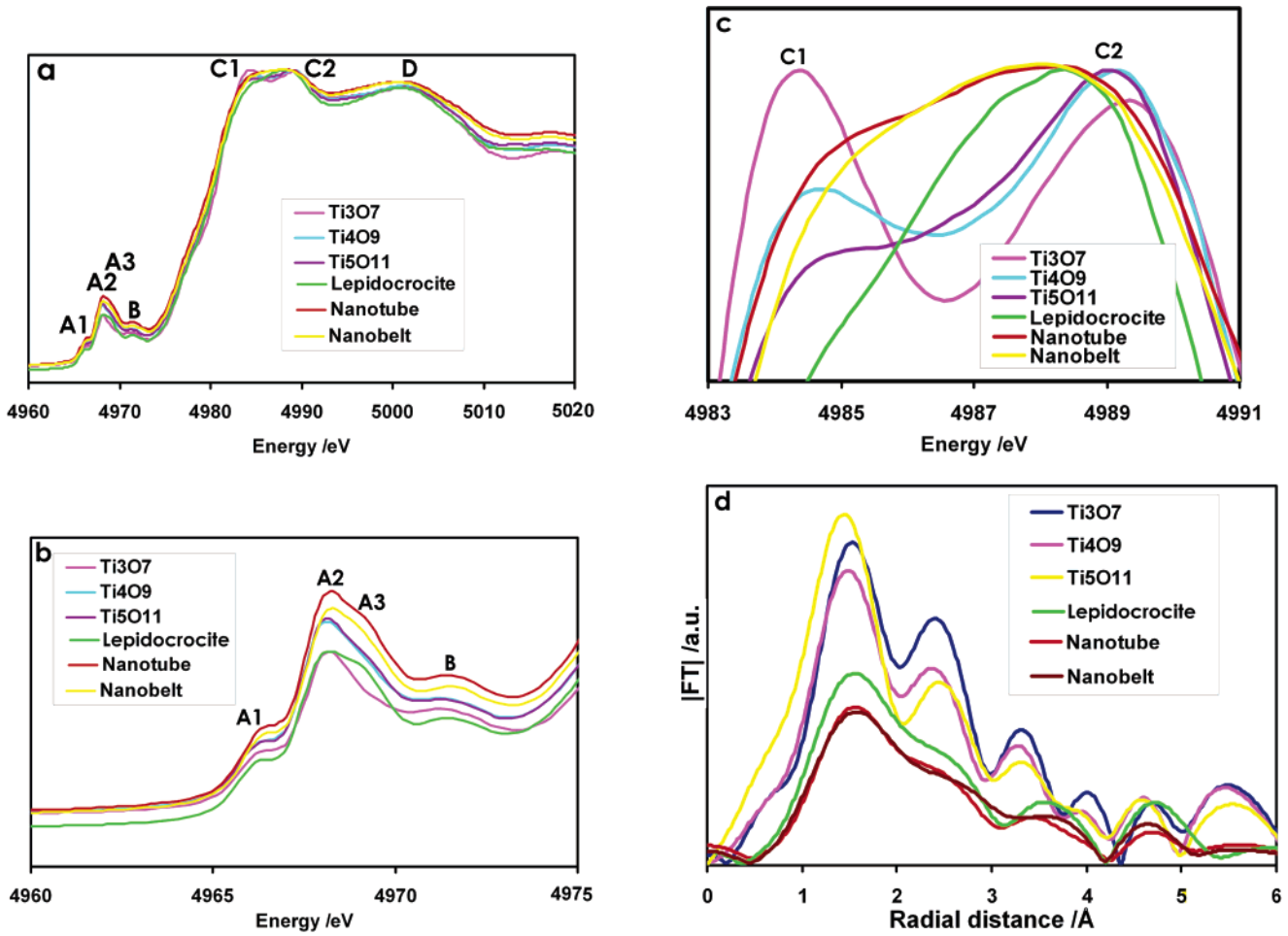

Figure 4. XAFS of nanotubes/nanobelts in comparison with other layered titanates: (a) XANES spectra; (b) enlarged pre-edge regions; (c) enlarged white line regions; and (d) RDA functions.

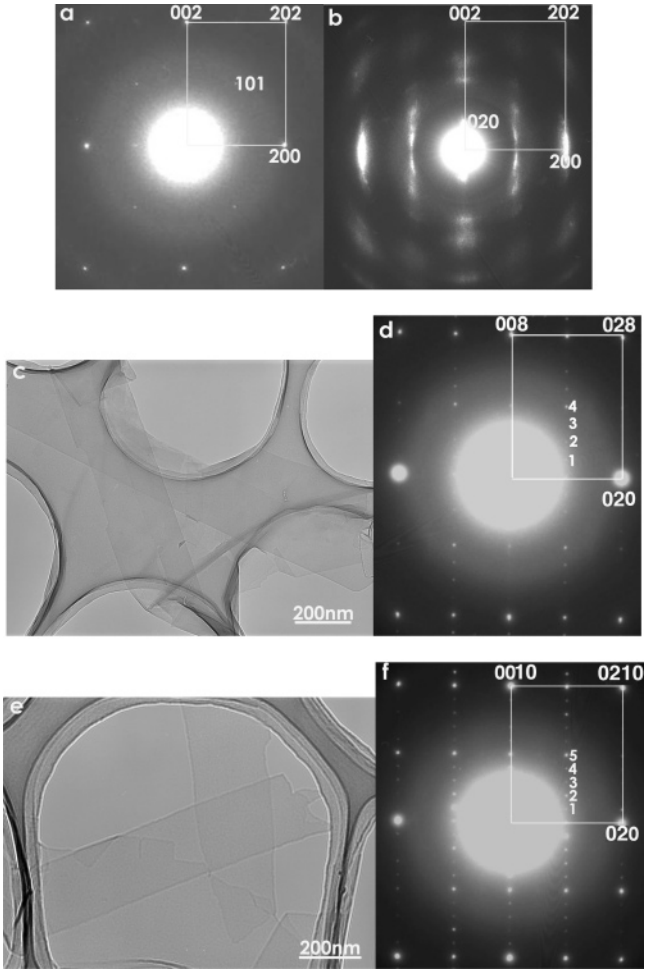

Figure 5. ED characterizations of nanotubes and nanosheets: (a) lepidocrocite nanosheet; (b) nanotubes; (c, d) TEM image of Ti_4O_9 nanosheet and corresponding ED pattern; and (e, f) TEM image of Ti_5O_{11} nanosheet and corresponding ED pattern. Note the orthogonal units of 0.38 nm × 0.30 nm in all the patterns.

eV, implying the splitting of the excitations from 1s to the molecular orbital of 4p. The intensity of the C1 peak gradually decreases in a sequence from Ti_3O_7, Ti_4O_9, to Ti_5O_{11}. On the other hand, lepidocrocite titanate does not exhibit an apparent C1 peak. As Ti_3O_7, Ti_4O_9, and Ti_5O_{11} sheets are periodically stepped of 3, 4, 5 octahedra wide, respectively, whereas the layers of lepidocrocite are not stepped but continuous in two dimensions, it seems that the steady reduction in the C1 peak intensity might be related to the edge-sharing octahedral width. As far as the C1/C2 peak features of nanotubes/nanobelts are concerned, they show some intermediate stage between Ti_3O_7 and lepidocrocite. Figure 4d displays the radial distribution of the atoms (RDA) function of different titanates. The almost identical peak positions and intensities can be clearly observed for nanotubes/nanobelts and lepidocrocite, indicating a very similar nearest neighboring environment. Judging from the RDA, the local structure of nanotubes/nanobelts might be closer to that of lepidocrocite than stepped titanates.

Finally, the electron diffraction (ED) patterns of nanotubes/nanobelts are compared with those of different titanate nanosheets. As they generally lay flat on the copper grid perpendicular to the electron beam, the ED patterns reflect the in-layer structure of the titanates. As we previously reported, the ED pattern of a single-layer lepidocrocite sheet projected along the sheet normal displays a typical orthogonal unit of 0.38 nm × 0.30 nm (Figure 5a).[14] In contrast, the patterns of nanotubes exhibit layered basal

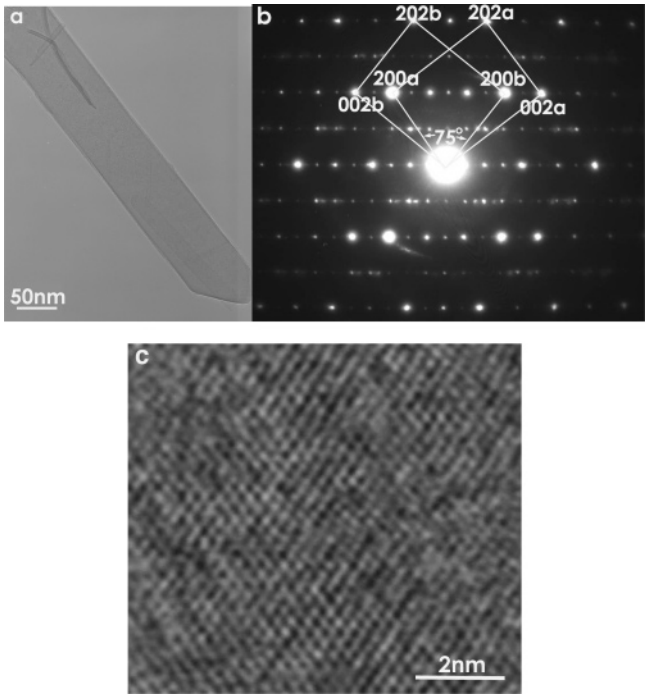

Figure 6. (a) Typical nanobelt; (b) ED pattern showing the twin structure with 75° inclining angle; (c) HRTEM image of the nanobelts showing continuous lattices without the twin boundary.

series in addition to the orthogonal unit, reflecting a peculiar multilayer tubular morphology.[20] A particular indexation of the pattern to the lepidocrocite structure is shown in Figure 5b. Analogous to the interpretation of XRD patterns, if monoclinic steeped titanates of $A_2Ti_nO_{2n+1}$ ($n = 3, 4, 5$) are assumed, the indices should be accordingly changed. For comparison, the morphologies and ED patterns of single-layer nanosheets of Ti_4O_9 and Ti_5O_{11} were obtained as shown in Figure 5c−f. A repeating structural unit, corresponding to a diagonal length of the edge-shared 4, 5 octahedra, yields an array of diffraction spots along the c^*-axis. The pseudoperiodicity of 0.38 nm × 0.30 nm subunits induces a modulation effect, resulting in the repetitive enhancement of the diffraction intensity of every 4, 5 spot in Ti_4O_9 and Ti_5O_{11}, respectively. Though the single-layer Ti_3O_7 nanosheet is not obtained, a repetition of intensity enhancement every 3 spots along the c^*-axis is reasonably expected for an ED pattern projecting to the sheet normal. As this modulation phenomenon is not observed in the ED pattern of nanotubes, it evidences that the nanotubes might be constructed from lepidocrocite sheets.

Figure 6a shows an individual nanobelt. The corresponding ED pattern is given in Figure 6b. As the nanobelts are composed of a few stacked titanate layers, the pattern was supposed to display a similar orthogonal subunit of 0.38 nm × 0.30 nm. However, this orthogonal unit is not obvious as in nanotubes and nanosheets. Instead, two identical 0.38 nm × 0.30 nm units with an inclination angle of 75° could be indexed in Figure 6b. The existence of two identical units indicates a possible twin structure inclined by 75°, either in-layer or inter-layer. However, the examinations of the HRTEM images of the nanobelts showed continuous lattice fringes without any twin defect or boundary at all (Figure 6c). The exact structure interpretation still needs further study.

Conclusion

High-purity nanotubes and nanobelts were almost isolated in simple hydrothermal procedures with different treating

temperatures and durations. Their structure features were investigated by XRD, Raman, XAFS, and ED measurements in comparison with known layered titanates. It reveals that both the nanotubes and nanobelts might be of layered titanate structure origin. This work offers a viewpoint for controllable synthesis of titanate nanotubes and nanobelts. It also contributes to clarify the current controversy on the structures of hydrothermally synthesized titanate nanomaterials.

Acknowledgment. This work was supported by CREST of the Japan Science and Technology Agency (JST). The XAFS measurements were performed under the approval of the Photon Factory Program Advisory Committee (2003G270).

References and Notes

(1) Anderson, S.; Wadsley, A. D. *Acta Crystallogr.* **1961**, *14*, 1245.
(2) Verbaere, A.; Tournoux, M. *Bull. Soc. Chim. Fr.* **1973**, 1237.
(3) Dion, M.; Piffard, Y.; Tournoux, M. *J. Inorg. Nucl. Chem.* **1978**, *40*, 917.
(4) Grey, I. E.; Madsen, I. C.; Watts, J. A.; Bursill, L. A.; Kwiatkowska, J. *J. Solid State Chem.* **1985**, *58*, 350.
(5) Anderson, S.; Wadsley, A. D. *Acta Crystallogr.* **1962**, *15*, 194.
(6) Sasaki, T.; Fujiki, Y. *J. Solid State Chem.* **1989**, *83*, 45.
(7) Sasaki, T.; Watanabe, M.; Fujiki, Y.; Kitami, Y. *Chem. Mater.* **1994**, *6*, 1749.
(8) Marchand, R.; Brohan, L.; Tournoux, M. *Mater. Res. Bull.* **1980**, *15*, 1129.
(9) Sasaki, T.; Watanabe, M.; Komatsu, Y.; Fujiki, Y. *Inorg. Chem.* **1985**, *24*, 2265.
(10) Sasaki, T.; Komatsu, Y.; Fujiki, Y. *Chem. Mater.* **1992**, *4*, 894.
(11) Grey, I. E.; Li, C.; Madsen, I. C.; Watts, J. A. *J. Solid. State Chem.* **1987**, *66*, 7.
(12) Sasaki, T.; Watanabe, M.; Michiue, Y.; Komatsu, Y.; Izumi, F.; Takenouchi, S. *Chem. Mater.* **1995**, *7*, 1001.
(13) Sasaki, T.; Watanabe, M. *J. Am. Chem. Soc.* **1998**, *120*, 4682.
(14) Sasaki, T.; Watanabe, M. *J. Phys. Chem. B* **1997**, *101*, 10159.
(15) Kasuga, T.; Hiramatsu, M.; Hoson, A.; Sekino, T.; Niihara, K. *Langmuir* **1998**, *14*, 3160.
(16) Kasuga, T.; Hiramatsu, M.; Hoson, A.; Sekino, T.; Niihara, K. *Adv. Mater.* **1999**, *11*, 1307.
(17) Chen, Q.; Du, G. H.; Zhang, S.; Peng, L. M. *Acta Crystallogr. B* **2002**, *58*, 587.
(18) Tian, Z. R.; Voigt, J. A.; Liu, J.; Mckenzie, B.; Xu, H. *J. Am. Chem. Soc.* **2003**, *125*, 12384.
(19) Yao, B. D.; Chan, Y. F.; Zhang, X Y.; Zhang, W. F.; Yang, Z. Y.; Wang, N. *Appl. Phys. Lett.* **2003**, *82*, 281.
(20) Ma, R.; Bando, Y.; Sasaki, T. *Chem. Phys. Lett.* **2003**, *380*, 577.
(21) Yang, J. J.; Jin, Z. S.; Wang, X. D.; Li, W.; Zhang, J. W.; Zhang, S. L.; Guo, X. Y.; Zhang, Z. J. *Dalton Trans.* **2003**, 3898.
(22) Yuan, Z. Y.; Colomer, J. F.; Su, B. L. *Chem. Phys. Lett.* **2002**, *363*, 362.
(23) Balachandran, U.; Eror, N. G. *J. Solid State Chem.* **1982**, *42*, 276.
(24) Sasaki, T.; Nakano, S.; Yamauchi, S.; Watanabe, M. *Chem. Mater.* **1997**, *9*, 602.
(25) Bamberger, C. E.; Begun, G. *J. Am. Ceram. Soc.* **1987**, *70*, C-48.
(26) Kim, H. M.; Miyaji, F.; Kokubo, T. *J. Mater. Sci.: Mater. Med.* **1997**, *8*, 341.
(27) Kudo, A.; Kondo, T. *J. Mater. Chem.* **1997**, *7*, 777.
(28) Fukuda, K.; Nakai, I.; Oishi, C.; Nomura, M.; Harada, M.; Ebina, Y.; Sasaki, T. *J. Phys. Chem. B* **2004**, *108*, 13088.